

Probing cosmic star formation up to $z = 9.4$ with GRBs

E. E. O. Ishida^{1,2,3*}; R. S. de Souza^{1,3}, A. Ferrara^{4,1}

¹*IPMU, University of Tokyo, 5-1-5 Kashiwanoha, Kashiwa, Chiba 277-8568, Japan*

²*Max-Planck-Institut für Astrophysik, Karl-Schwarzschild-Str. 1, D-85748 Garching, Germany*

³*Excellence Cluster Universe, Technische Universität München, Boltzmannstrasse 2, 85748 Garching, Germany*

⁴*Scuola Normale Superiore, Piazza dei Cavalieri 7, 56126 Pisa, Italy*

Accepted – Received –

ABSTRACT

We propose a novel approach, based on Principal Components Analysis, to the use of Gamma-Ray Bursts (GRBs) as probes of cosmic star formation history (SFH) up to very high redshifts. The main advantage of such approach is to avoid the necessity of assuming an *ad hoc* parameterization of the SFH. We first validate the method by reconstructing a known SFH from Monte Carlo-generated mock data. We then apply the method to the most recent *Swift* data of GRBs with known redshift and compare it against the SFH obtained by independent methods. The main conclusion is that the level of star formation activity at $z \approx 9.4$ could have been already as high as the present-day one ($\approx 0.01 M_{\odot} \text{ yr}^{-1} \text{ Mpc}^{-3}$). This is a factor 3-5 times higher than deduced from high- z galaxy searches through drop-out techniques. If true, this might alleviate the long-standing problem of a photon-starving reionization; it might also indicate that galaxies accounting for most of the star formation activity at high redshift go undetected by even the most deep searches.

Key words: methods: statistical, gamma-ray burst, star formation

1 INTRODUCTION

The cosmic star formation history (SFH) is an important test for galaxy formation models. Experimentally our knowledge of the SFH comes from Hopkins & Beacom (2006) up to $z \approx 6$ and from observations of color-selected Lyman Break Galaxies (Mannucci et al. 2007; Bouwens et al. 2008), Ly α Emitters (Ota et al. 2008), UV+IR measurements (Reddy et al. 2008), and GRB observations (Chary et al. 2007; Yüksel et al. 2008; Wang & Dai 2009) at higher z (hereafter, these will be referred to as H2006, M2007, B2008, O2008, R2008, C2007, Y2008 and W2009, respectively). However, direct high- z measurements constitute an extreme challenge even for the most powerful telescopes and remain sparse.

Due to their high luminosity GRBs can be used as SFH probes into the very distant Universe (Lamb & Reichart 2000; Porciani & Madau 2001; Bromm & Loeb 2002; Totani et al. 2006; Fynbo et al. 2006; Price et al. 2006; Savaglio 2006; Prochaska et al. 2007; Li 2008; de Souza et al. 2011), potentially to higher redshifts than allowed by galaxies alone. For example, GRB 090429B at $z = 9.4$ (Cucchiara et al. 2011) is the current record-holder object, followed by a $z = 8.6$ galaxy (Lehnert et al. 2010)

and GRB 090423, at $z = 8.26$ (Salvaterra et al. 2009; Tanvir et al. 2009).

In principle, the redshift distribution of GRBs can give us important clues on the early stages of cosmic history. In practice, the connection between GRBs and the underlying host galaxy star formation mode is far from trivial (see e.g. Kocevski et al. (2009)), thus making the probe value subject to uncertainties.

The purpose of this work is to show how *Principal Component Analysis* (PCA) can be used to map the GRB redshift distribution onto the cosmic SFH in a model-independent way. PCA has already been applied to other astrophysical and cosmological contexts (Huterer & Starkman 2003; Maturi & Mignone 2009; Mitra et al. 2010; Ishida & de Souza 2011), and recognized as a useful tool to reconstruct parameters without the introduction of *ad hoc* parameterizations¹.

2 THEORETICAL GRB RATE

We assume that the formation rate of long GRBs (duration longer than 2 sec) follows closely the SFH

¹ Throughout the paper we adopt a Λ CDM model with WMAP7 best fit parameters (Jarosik et al. 2011), $\Omega_m = 0.267, \Omega_{\Lambda} = 0.734$, and $H_0 = 71 \text{ km s}^{-1} \text{ Mpc}^{-1}$.

* e-mail: emille.ishida@ipmu.jp (EEOI)

(e.g., Totani (1997); Campisi et al. (2010); Ciardi & Loeb (2000); Campisi et al. (2011); Conselice et al. (2005); Bromm & Loeb (2006); de Souza et al. (2011)). Hence, the comoving rate of observable GRBs, Ψ_{GRB} is

$$\Psi_{\text{GRB}}(z) = (\Omega_{\text{obs}}/4\pi) f_{\text{GRB}} f_b P_z \rho_*(z) \int_{\log L_{\text{lim}}(z)}^{\infty} \Phi(L) d \log L, \quad (1)$$

where Ω_{obs} is the field of view of the experiment, f_{GRB} is the GRB formation efficiency, f_b is the beaming factor of the burst, P_z is the fraction of GRBs with measured redshift and $L_{\text{lim}}(z)$ is the luminosity threshold of a given experiment. In the following we discuss in detail each of the terms in eq. (1).

We define telescope-related quantities in eq. (1) after *Swift* specs, i.e. $\Omega_{\text{obs}} = 1.4$ (Salvaterra et al. 2008) and $P_z = 0.24 \pm 0.06$.² The overall GRB rate depends on $f_b \approx \theta^2/2$, where θ is the opening angle of the jet. According to Guetta et al. (2005) the average value of $f_b = 0.01 - 0.02$. Using a radio transients survey, Gal-Yam et al. (2006) placed the upper limit $f_b \lesssim 0.016$. We set $f_b = 0.013 \pm 0.003$ as a fiducial value.

The stellar Initial Mass Function (IMF), $\phi(m)$, determines the fraction of stars massive enough to leave a black hole remnant. Current theories indicate that the threshold mass to trigger a GRB is $M_{\text{GRB}} = 25M_{\odot}$ (Bromm & Loeb 2006). However, only a fraction $\zeta_{\text{GRB}} \approx 10^{-3}$ (Langer & Norman 2006) of black holes resulting from supernova explosion actually gives rise to a GRB; to be conservative, we considered $\zeta_{\text{GRB}} = (1.0 \pm 0.5) \times 10^{-3}$. Hence, the GRB formation efficiency factor per stellar mass is

$$f_{\text{GRB}} = \zeta_{\text{GRB}} \frac{\int_{M_{\text{GRB}}}^{M_{\text{up}}} \phi(m) dm}{\int_{M_{\text{low}}}^{M_{\text{up}}} m \phi(m) dm}. \quad (2)$$

For simplicity, we assume a ‘‘standard’’ Salpeter IMF, $\phi(m) \propto m^{-2.35}$, with $(M_{\text{low}}, M_{\text{up}}) = (0.1M_{\odot}, 100M_{\odot})$ (Schneider et al. 2006).

The number of detectable GRBs depends on the instrument sensitivity and intrinsic isotropic GRB luminosity function. For the latter, we adopt a power-law distribution function of Wanderman & Piran (2010)

$$\Phi(L) = \begin{cases} (L/L_*)^{-\alpha_L} & L < L_*, \\ (L/L_*)^{-\beta_L} & L > L_*. \end{cases}, \quad (3)$$

with $L_* = 10^{52.5} \text{ erg s}^{-1}$, $\alpha_L = 0.2_{-0.1}^{+0.2}$ and $\beta_L = 1.4_{-0.6}^{+0.3}$. The luminosity threshold is then $L_{\text{lim}} = 4\pi d_L^2 F_{\text{lim}}$, where d_L is the luminosity distance and F_{lim} is the bolometric energy flux limit of the instrument. In what follows we set $F_{\text{lim}} = 1.2 \times 10^{-8} \text{ erg cm}^{-2} \text{ s}^{-1}$ (Li 2008).

From eq. (1) we can determine the number of observed GRBs with redshift in $(z, z + dz)$ over a time interval, Δt , in the observer rest frame:

$$\frac{dN_{\text{GRB}}}{dz} = \Psi_{\text{GRB}}(z) \frac{\Delta t}{1+z} \frac{dV}{dz}, \quad (4)$$

where dV/dz is the comoving volume element per unit of redshift.

Our observable, i.e. the cumulative number $N(z)$ of GRBs up to redshift z , is given by

$$N(z) = \int_0^z \frac{dN_{\text{GRB}}}{dz'} dz'. \quad (5)$$

So far we have discussed the physical meaning of all terms in eq. (1) except the SFH. Since our aim is to build a model which is independent from the specific form of $\rho_*(z)$, we avoid making hypothesis about this quantity. Instead, our intention is to derive $\rho_*(z)$ by using PCA and a (mock or real) data set whose data points are $\{z_i, N(z_i)\}$ pairs.

3 PRINCIPAL COMPONENT ANALYSIS

The main goal of PCA is the dimensionality reduction of an initial parameter space through the analysis of its internal correlations. Suppose we have a model composed by P parameters. If two of them are highly correlated, they are actually providing the same information. This means that it is possible to rewrite the data in a new parameter space consisting of $P - 1$ terms, with minimum loss of information (for a complete review see Jolliffe (2002)). This new set of parameters are recognized as the principal components (PCs), or the eigenvectors of the Fisher information matrix, \mathbf{F} .

We postulate that the data set is composed by N independent observations, each one characterized by a Gaussian probability density function, $f_i[g(x_i, \boldsymbol{\beta}); G_i, \sigma_i]$. In our notation, x_i is a measurement of an independent variable; G_i represent the measurements of a quantity G depending on x_i ; σ_i is the uncertainty associated with the measures, and $\boldsymbol{\beta}$ is the parameter vector of the theoretical model. In other words, we investigate a specific quantity, g , which can be written as a function of the parameters β_i . In this context, the likelihood function is given by $\mathcal{L} = \prod_{i=1}^N f_i$ and the Fisher matrix is defined as

$$F_{kl} \equiv \left\langle -\frac{\partial^2 \ln L(\boldsymbol{\beta})}{\partial \beta_k \partial \beta_l} \right\rangle. \quad (6)$$

Brackets in eq. (6) represent the expectation value.

We can now diagonalize \mathbf{F} , and determine the set of its eigenvectors/PCs, \mathbf{e} , and eigenvalues, $\boldsymbol{\lambda}$. Following the standard convention, we enumerate \mathbf{e}_i from the largest to the smallest associated eigenvalue. Our ability to determine the form of each PC is given by $\sigma_{\text{PC}_i} = \lambda_i^{-1/2}$.

The set \mathbf{e} forms a complete base of uncorrelated vectors. This allows us to use a subspace of \mathbf{e} , \mathbf{eM} , to rewrite g as a linear combination of all the elements in \mathbf{eM} , $g_{\text{rec}}(x, \boldsymbol{\alpha})$. The data is then used to find the values of the linear expansion coefficients, $\boldsymbol{\alpha}$ (for a detailed discussion see I2011).

The question of how many PCs should be used in the final reconstruction, or how to choose the dimensionality of \mathbf{eM} , depends on the particular data set analyzed and our expectation towards them. To provide an idea of how much of the initial information (variance) is included in our plots, we shall order them following their *cumulative percentage of total variance*. A reconstruction with the first M PCs

² Following Wanderman & Piran (2010) we consider redshift measurements obtained via absorption and photometry only. For further details see Sec. 4.

encloses a percentage of this value

$$t_M = 100 \frac{\sum_{i=1}^M \lambda_i}{\sum_{j=1}^P \lambda_j}. \quad (7)$$

It is important to emphasize that each added PC brings its associated uncertainty (σ_{PC_i}) into the reconstruction. So, although the best-fitted reconstruction converges to the “real” function as M increases³, the uncertainty associated also raises. As a consequence, the question of how many PCs turns into a matter of what percentage of total variance we are willing to enclose.

3.1 Star formation history from GRB distribution

To specify our method of SFH reconstruction from GRB data, let us consider a data set formed by T measurements of the cumulative number of GRB up to redshift z_i , $N_{data_i} = N(z_i)$, and its corresponding uncertainty (σ_i). The likelihood is given by

$$\mathcal{L}(\boldsymbol{\beta}) \propto \prod_{i=1}^T \exp \left[-\frac{1}{2} \left(\frac{N_{data_i} - N(z_i, \boldsymbol{\beta})}{\sigma_i} \right)^2 \right]. \quad (8)$$

Using equation (6), the Fisher matrix components are

$$F_{k,l} = \sum_{i=1}^T \frac{1}{\sigma_i^2} \frac{\partial N(z_i, \boldsymbol{\beta})}{\partial \beta_k} \frac{\partial N(z_i, \boldsymbol{\beta})}{\partial \beta_l}. \quad (9)$$

The Fisher matrix determination is now a matter of calculating the derivatives of $N(z, \boldsymbol{\beta})$, for which we use the theoretical prescriptions of Sec. 2. Aiming at model independence and simplicity, we model the SFH as

$$\rho_*(z, \boldsymbol{\beta}) = \sum_{i=1}^{n_{\text{bin}}} \beta_i c_i(z), \quad (10)$$

where β_i are constants, n_{bin} is the total number of redshift bins, and $c_i(z)$ is a window function which returns 1 if $z_i < z \leq z_{i+1}$ and 0 otherwise. Using this description, we may write any functional form with resolution limited by our computational power.

The derivatives of $N(z)$ can be computed analytically:

$$\frac{\partial N(z, \boldsymbol{\beta})}{\partial \beta_k} = H(J(z) + 1 - k) \left[\sum_{i=1}^{J(z)} \delta_{k,i} A(z l_i, z l_{i+1}) + \delta_{k, J(z)+1} A(z l_{J(z)+1}, z) \right], \quad (11)$$

where $H(x)$ is a step function which returns 0 if $x < 0$ and 1 otherwise, $J(z)$ corresponds to the number of integer bins up to redshift z , $\delta_{i,j}$ is the Kronecker delta function, $z l_i$ is the lower bound of the i -th redshift bin, and

$$A(z_1, z_2) \equiv \frac{\Omega_{\text{obs}} \Delta t}{4\pi} f_b f_{\text{GRB}} P_z \times \int_{z_1}^{z_2} \frac{1}{(1+x)} \frac{dV}{dz}(x) \int_{\log L_{\text{lim}}(x)}^{\infty} \Phi(L) d \log L dx. \quad (12)$$

³ This limit holds in ideal situations, where the number of data points largely exceeds the number of initial parameters. If the data set is small or approximately the same size of the initial parameter space, one should also care for overfitting problems.

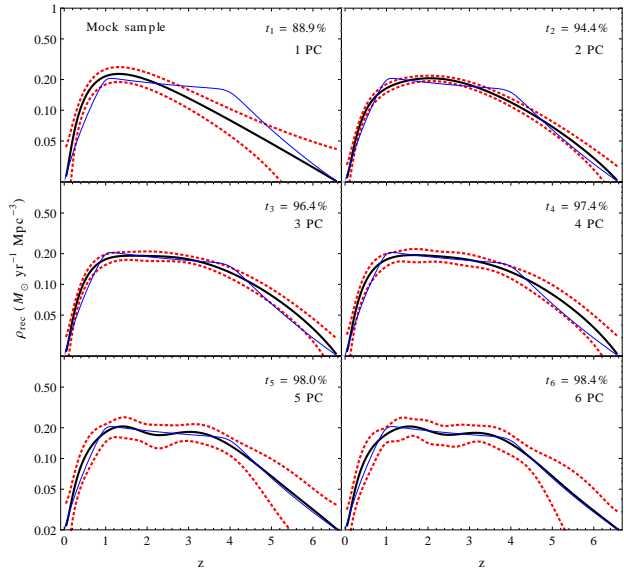


Figure 1. PCA reconstructions of SFH obtained from our mock data, using 1 (top-left) to 6 (bottom-right) PCs. The blue-thin line corresponds to our fiducial model ρ_{fid} . The black-thick line is the final reconstruction for each case and the red-dashed-thick lines corresponds to 2σ confidence levels. The inset shows the cumulative percentage of total variance, t_M .

From these relations the Fisher matrix can be computed and the functional form of the SFH reconstructed through PCA.

4 RECONSTRUCTION

Mock data The mock sample is composed of data pairs $\{z_i, N(z_i)\}$, distributed in redshift bins of width $\Delta z = 0.1$, where z_i represents the middle of each bin. The fiducial model used for the SFH is a simple double-exponential function, ρ_{fid} , fitted to numerical results by Li (2008),

$$\log \rho_{\text{fid}}(z) = a + b \log(1 + z), \quad (13)$$

with $(a, b) = (-1.70, 3.30)$ for $z < 0.993$; $(-0.727, 0.0549)$ for $0.993 < z < 3.80$ and $(2.35, -4.46)$ for $z > 3.80$. We generated 500 simulations, each realization with uncertainty in the determination of $N(z)$ set to unit and containing 65 redshift bins. After we generated the mock sample, the information about $\rho_{\text{fid}}(z)$ is discarded. Our goal from now on is to re-obtain the functional form of eq. (13) from PCA.

The Fisher matrix is obtained as described above, assuming an observing time $\Delta t_{\text{MS}} = 1$ yr. As the mock sample purpose is to test the procedure under an ideal scenario, we did not include uncertainties in the parameters of eq. (1). Having obtained the PCs, we can rewrite the SFH as

$$\rho_{\text{rec}}(z) = \rho_c + \sum_{i=1}^M \alpha_i \mathbf{e}_i(z), \quad (14)$$

where α_i and ρ_c are constants to be determined and M is the number of PCs we choose to use in the reconstruction. The simulated data points are then used to find the appropriate values for the parameters α_i and ρ_c as those that minimize

the expression

$$\chi^2(\boldsymbol{\alpha}) \propto \sum_{i=1}^{T_{\text{MS}}} \frac{(N_{i;\text{data}} - N_{\text{rec}}(z_i; \rho_c, \boldsymbol{\alpha}))^2}{2\sigma_i^2}, \quad (15)$$

where $\sigma_i = 1$ for all redshift bins. The reconstructions obtained using 1 to 6 PCs are shown in Fig. 1. The uncertainty in the final reconstruction was calculated by a quadrature sum that includes the parameters σ_{PC_i} and the uncertainty in the determination of parameters $\boldsymbol{\alpha}(\sigma_{\alpha_i})$ and $\rho_c(\sigma_{\rho_c})$.

From Fig. 1 we can appreciate the success of the procedure in reconstructing the underlying unknown SFH in an ideal scenario, with increasing agreement as the number of PCs raises. Confidence levels also become wider as M increases, with the only exception of the reconstruction with 1 PC. Since σ_{ρ_c} dominates the errors due to the limited freedom to fit the second peak of the fiducial model with only 1 PC. With 2 PCs fitting the second peak becomes easier, and as a consequence, the magnitude of σ_{ρ_c} decreases to levels below those of σ_{PC_1} .

Swift data After validating PCA reconstruction under ideal conditions, we turn to the use of currently available *Swift* data, and compare these results with independent measurements of SFH from the literature. First, we need to properly choose our data set. Since only GRBs with measured redshifts can be used in our analysis, the question of how the redshift measurements were obtained must be examined carefully.

GRBs redshifts are generally obtained from optical afterglow spectra using absorption lines or photometry, or from the spectrum of the host galaxy using emission lines. As pointed by Wanderman & Piran (2010), different methods yield different redshift distributions: a visual inspection of Fig. 2 illustrates this point. Most noticeably, the GRB redshift distribution determined from their hosts lacks very high- z events. Moreover, emission (and to a lesser extent, absorption) lines are susceptible to a selection effect known as the “redshift desert” in the range $1.1 < z < 2.1$ (Fiore et al. 2007; Coward 2009). Additional bias sources are preliminary discussed by Malesani et al. (2009). To avoid systematic errors affecting the overall redshift distribution, our data sample is composed by 120 *Swift* GRBs with redshift determined from absorption lines and photometry (gray region in Fig. 2, top panel).

The next step is to choose the appropriate redshift bin width. In principle, the quality of the reconstruction should increase with the number of bins. However, as GRB are discrete events, if we pick a bin width based on the available data (for example, in such a way that each bin has at least one GRB), the bins will be too wide (≈ 1). In this case, the assumption that the SFH is constant inside the bin will not hold, leading to reconstructions with bad resolution. To overcome this limitation we performed a gaussian kernel fit⁴ to the data (black line in Fig. 2, top panel). Now we have a continuous probability distribution function (PDF) for dN/dz , which follows the real data distribution and al-

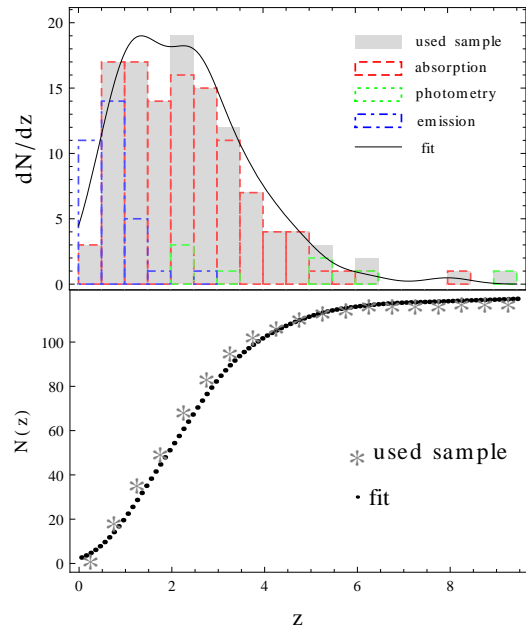


Figure 2. **Top:** Histogram showing the measured redshift distribution of 120 GRBs detected by *Swift* from 2005 to 2010, divided by redshift measurement methods: absorption (red-dashed), photometry (green-dotted) and emission (blue-dot-dashed). The gray region corresponds to the redshift distribution of data we used (absorption + photometry). The solid black line shows the fit to the used data distribution. **Bottom:** The cumulative distributions constructed from *Swift* data (gray stars) and from our fitted distribution function (black points).

lows us to set the bin width as small as required. We kept $\Delta z = 0.1$ and use the PDF to calculate the cumulative number of observed GRBs in each bin. The comparison between the real data cumulative distribution and the one calculated via the fitted PDF are shown in Fig. 2, bottom panel.

The Fisher matrix is calculated using $\Delta t_{\text{sw}} = 6$ yr of observation time. The parameters σ_i were obtained by summing in quadrature the uncertainties in the quantities involved in eq. (1). Fig. 3 shows the first 2 PCs and the corresponding reconstruction using both of them, which already encloses more than 97% of total variance. In the lower panel, the points correspond to completely independent measurements from the literature. These data points are shown only for comparison purposes and have not been used in our calculations.

5 DISCUSSION

We have proposed the use of PCA as a powerful tool to reconstruct the cosmic star formation history exploiting the measured gamma-ray burst redshift distribution. The procedure was successfully validated using synthetic data and next applied to actual *Swift* data (Fig. 3).

It is important to highlight that the approach is completely independent of the initial choice of the theoretical model parameter vector, $\boldsymbol{\beta}$. This has the obvious advantage of avoiding any a priori hypothesis on the SFH, $\rho_*(z)$. However, the degeneracy between $\rho_*(z)$ and any other factor we are failing to take into account cannot be removed, i.e.

⁴ A non-parametric estimate of the PDF obtained from a linearly interpolated version of $\frac{1}{nh} \sum_{i=1}^n k\left(\frac{x-x_i}{h}\right)$ for a kernel $k(x)$, bin width h and a total of n bins.

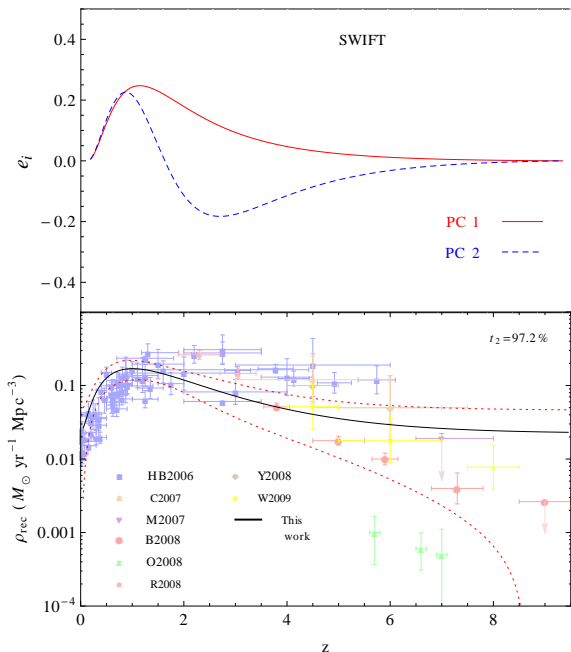


Figure 3. **Top:** First (red solid) and second (blue dashed) PCs from *Swift*. **Bottom:** PCA reconstruction from *Swift* data using 2 PCs, compared with independent SFH determinations (light points, not used in our calculations). The black solid line is the PCA best-fit reconstruction using 2 PCs; the red dashed lines correspond to 2σ confidence levels. The inset shows the cumulative percentage of total variance, t_M .

the reconstructed SFH contains also the behavior of all the agents influencing the determination of $N(z)$ and not included in the model.

For example, Langer & Norman (2006); Woosley & Heger (2006) have argued that GRB progenitors will have a low metallicity. Such an effect would be a consequence of the mass and angular momentum loss caused by winds in high-metallicity stars. This would prevent such stars of becoming GRBs and consequently, change their expected redshift distribution (Salvaterra & Chincarini 2007; Salvaterra et al. 2007; Li 2008). We implicitly considered that this and other such effects will span within the error bars in our analysis.

In spite of the remaining uncertainties, which are probably less severe than those affecting other methods aimed at recovering the high- z tail of the SFH, there are robust indications that we can gather from the analysis of our results. The first is that the combination of GRB data and PCA suggest that the level of star formation activity at $z \approx 9.4$ could have been already as high as the present-day one ($\approx 0.01 M_{\odot} \text{ yr}^{-1} \text{ Mpc}^{-3}$). This is a factor 3-5 times higher than deduced from high- z galaxy searches through drop-out techniques, similarly to the trend found by Yonetoku et al. (2004). If true, this might alleviate the long-standing problem of a photon-starving reionization; it might also indicate that galaxies accounting for most of the star formation activity at high redshift go undetected by even the most deep searches. Finally it is worth noticing that a sustained high- z star formation activity is consistent with predictions of reionization models that simultaneously match a number of observable experimental constraints as the Gunn-Peterson effect, Thom-

son free-electron optical depth, Lyman Limit Systems statistics etc. (Choudhury & Ferrara (2006), Bolton & Haehnelt (2007)). Given the expected large growth of GRB detections from the next generation of instruments, the method proposed here promises to become one of the most suitable and reliable tools to constrain the star formation activity in the young Universe.

ACKNOWLEDGEMENTS

We thank K. Ioka, R. Salvaterra and N. Yoshida for useful comments. E.E.O.I. thanks CAPES (1313-10-0) for financial support. R.S.S. thanks CNPq (200297/2010-4) for financial support. AF acknowledges support from IPMU where this research started. This work was supported by WPI Initiative, MEXT, Japan.

REFERENCES

- Bolton J. S., Haehnelt M. G., 2007, *MNRAS*, 381, L35
 Bouwens R. J., et al. 2008, *ApJ*, 686, 230
 Bromm V., Loeb A., 2002, *ApJ*, 575, 111
 Bromm V., Loeb A., 2006, *ApJ*, 642, 382
 Campisi M. A., Li L.-X., Jakobsson P., 2010, *MNRAS*, 407, 1972
 Campisi M. A., Maio U., Salvaterra R., Ciardi B., 2011, ArXiv e-prints
 Chary R., Berger E., Cowie L., 2007, *ApJ*, 671, 272
 Choudhury T. R., Ferrara A., 2006, *MNRAS*, 371, L55
 Ciardi B., Loeb A., 2000, *ApJ*, 540, 687
 Conselice C. J., Vreeswijk P. M., Fruchter A. S., Levan A., Kouveliotou C., Fynbo J. P. U., Gorosabel J., Tanvir N. R., Thorsett S. E., 2005, *ApJ*, 633, 29
 Coward D. M., 2009, *MNRAS*, 393, L65
 Cucchiara A., et al. 2011, arXiv:astro-ph/1105.4915
 de Souza R. S., Yoshida N., Ioka K., 2011, arXiv:astro-ph/1105.2395
 Fiore F., et al. 2007, *A&A*, 470, 515
 Fynbo J. P. U., et al. 2006, *A&A*, 451, L47
 Gal-Yam A., et al. 2006, *ApJ*, 639, 331
 Guetta D., Piran T., Waxman E., 2005, *ApJ*, 619, 412
 Hopkins A. M., Beacom J. F., 2006, *ApJ*, 651, 142
 Huterer D., Starkman G., 2003, *Physical Review Letters*, 90, 031301
 Ishida E. E. O., de Souza R. S., 2011, *A&A*, 527, A49+
 Jarosik N., et al. 2011, *ApJS*, 192, 14
 Jolliffe I. T., 2002, *Principal component analysis*
 Kocovski D., West A. A., Modjaz M., 2009, *ApJ*, 702, 377
 Lamb D. Q., Reichart D. E., 2000, *ApJ*, 536, 1
 Langer N., Norman C. A., 2006, *ApJ*, 638, L63
 Lehnert M. D., et al. 2010, *Nature*, 467, 940
 Li L., 2008, *MNRAS*, 388, 1487
 Malesani D., et al. 2009, *ApJ*, 692, L84
 Mannucci F., et al. 2007, *A&A*, 461, 423
 Maturi M., Mignone C., 2009, *A&A*, 508, 45
 Mitra S., Choudhury T. R., Ferrara A., 2010, arXiv:astro-ph/1011.2213
 Ota K., et al. 2008, *ApJ*, 677, 12
 Porciani C., Madau P., 2001, *ApJ*, 548, 522
 Price P. A., et al. 2006, *ApJ*, 645, 851
 Prochaska J. X., et al. 2007, *ApJ*, 666, 267

- Reddy N. A., et al. 2008, *ApJS*, 175, 48
Salvaterra R., et al. 2008, *MNRAS*, 385, 189
Salvaterra R., Campana S., Chincarini G., Tagliaferri G.,
Covino S., 2007, *MNRAS*, 380, L45
Salvaterra R., Chincarini G., 2007, *ApJ*, 656, L49
Salvaterra R., Della Valle M., Campana S., et al. 2009,
Nature, 461, 1258
Savaglio S., 2006, *New Journal of Physics*, 8, 195
Schneider R., et al. 2006, *MNRAS*, 369, 1437
Tanvir N. R., et al. 2009, *Nature*, 461, 1254
Totani T., et al. 2006, *PASJ*, 58, 485
Totani T., 1997, *ApJ*, 486, L71+
Wanderman D., Piran T., 2010, *MNRAS*, 406, 1944
Wang F. Y., Dai Z. G., 2009, *MNRAS*, 400, L10
Woosley S. E., Heger A., 2006, *The Astrophysical Journal*,
637, 914
Yonetoku D., et al. 2004, *ApJ*, 609, 935
Yüksel H., et al. 2008, *ApJ*, 683, L5

This paper has been typeset from a \TeX / \LaTeX file prepared by the author.